

Exact method of determination of the recombination mode from time resolved photoluminescence data

Pawel Strak¹, Kamil Koronski², Kamil Sobczak³, Jolanta Borysiuk⁴, Krzysztof P. Korona⁴, Konrad Sakowski¹, Andrzej Suchocki², Eva Monroy⁵, Stanislaw Krukowski¹, and Agata Kaminska^{2,6}

¹*Institute of High Pressure Physics, Polish Academy of Sciences, Sokolowska 29/37, 01-142 Warsaw, Poland*

²*Institute of Physics Polish Academy of Sciences, Aleja Lotnikow 32/46, PL-02-668 Warsaw, Poland*

³*Faculty of Chemistry, Biological and Chemical Research Centre, University of Warsaw, Zwirki i Wigury 101, 02-089 Warsaw, Poland*

⁴*Faculty of Physics, University of Warsaw, Pasteura 5, 02-093 Warsaw, Poland*

⁵*Université Grenoble-Alpes, CEA, INAC-Phelics, 17 av. des Martyrs, 38000 Grenoble, France*

⁶*Cardinal Stefan Wyszyński University, College of Science, Department of Mathematics and Natural Sciences, Dewajtis 5, 01-815 Warsaw, Poland*

A method of data analysis is proposed for the determination of the carrier recombination processes in optically excited matter measured by time-resolved photoluminescence, differentiating monomolecular, bi-molecular, tri-molecular, and higher order molecular processes. Our method allows to determine whether the so-called ABC model describes time evolution of optical relaxation of the excited system. The procedure is applicable to the time evolution of any optically excited medium. As an illustration, the method is successfully applied to III-nitride polar and non-polar multi-quantum wells. We show that in this case the mono- and bi-molecular processes determine the carrier relaxation, and the tri-molecular Auger recombination contribution is negligible.

PACS numbers: 73.21.Fg, 78.47.D-, 78.67.De, 78.55.Cr

I. INTRODUCTION

Photoluminescence (PL) and its time-resolved version (TRPL) are keystone characterization techniques to explore properties of systems as diverse as single atoms, molecules, solids, and a variety of quantum-confined structures, such as quantum wells, rods and dots. PL measurements probe the electronic states of the system [1,2]. As the amount of potential information is enormous, the PL measurement techniques steadily progress, extending their scope and functionalizing their application using different modifications and improvements [3]. Among the adopted features, TRPL is one of the most important and productive [3,4]. In TRPL measurements, optical excitation induces nonequilibrium occupation of a portion of quantum states, which then relax towards equilibrium. For extended systems, the nonequilibrium density of electrons and holes (e-h) is created by an initial laser pulse, and the excess of carriers relaxes by recombination. Part of the recombination processes entails emission of photons (i.e. radiative recombination) which are measured by optical detectors. The deexcitation processes without emission of photons contribute to non-radiative recombination. All the types of recombination may involve one, two, or more carriers; they are called mono-, bi-, tri-molecular, etc. processes. The time evolution of the excess carrier density may be studied by measurements of time evolution of the PL intensity. Solutions exist for each separate molecular type process, thus single processes can be distinguished easily [4]. In reality, several types of recombination can be entangled simultaneously and their deconvolution is difficult. Thus the direct and unambiguous PL time evolution analysis method does not exist in practice.

In practical analysis of the experimental results, it is assumed that the time decay of the optical emission of an excited semiconductor medium can be divided into monomolecular, bi-molecular, tri-molecular and possibly higher-order molecular processes [1-5]. It has to be also noted that division of the recombination channels into mono-, bi-, tri-, and higher molecular recombination modes does not entail precise identification of the nature of the recombination process. Thus, the monomolecular decay may contain contributions from several recombination modes, including nonradiative recombination, related to presence of defects, known as Shockley-Read-Hall (SRH) recombination [6], and also Wannier-Mott exciton recombination [7,8]. The contribution of single and collective excitons is dominant for low temperatures [9], i.e. at the conditions of majority of PL experiments. However, for high electron densities, excitons can be screened or even decomposed, so that they do not play

a dominant role [10,11]. Additionally, for recombination in multiquantum wells (MQWs), the escape from the wells may contribute to monomolecular decay [12]. Several physical mechanisms may lead to recombination outside QWs, including lack of electron capture in the wells, electron escape, asymmetry of electron and hole transport in semiconductors, etc. [13]. In many cases, additional experiments such as temperature or pressure dependent PL, in combination with *ab initio* calculations [14], are necessary to disentangle the different contributions to mono-molecular processes.

The radiative recombination, especially in semiconducting materials, may be related to band-to-band recombination, direct or indirect, which may be associated either with mono-molecular or bi-molecular recombination, depending on the condition of the experiment [15]. The observed PL time decay may be additionally affected by the energy transfer by exchange mechanisms, involving defects [16,17]. For example, the peculiar behavior of the PL intensity from $\text{In}_x\text{Ga}_{1-x}\text{N}$ ($0 < x < 0.25$) layers and MQWs was explained by Chichibu's localization model, according to which, the carrier are localized in high In content regions, and isolated from dislocations, which constitute the non-radiative recombination channels [18,19]. As it was confirmed experimentally [20,21], the localization works at low excitation, hence it is expected that at higher excitation, during the time evolution, the transition from non-localized to localized recombination mode may alter the results. In addition, the built-in and piezoelectric-induced electric fields in the wells [21-23] may affect the recombination by at least two different mechanisms: field-induced dissociation of the excitons and energy shift due to the screening of the electric field by photogenerated carriers [25].

The most prominent example of a tri-molecular or higher molecular process is Auger recombination. The process involves nonradiative transfer of the excess energy created due to e-h recombination to a third charge carrier (electron or hole), which is ejected from its original state [26,27]. Depending on the final state of the ejected carrier, several types of Auger processes were identified: internal, external, etc. Auger recombination was recently identified as the most likely phenomenon responsible for the efficiency droop in III-nitride light emitting diodes (LEDs) [28,29], i.e. the relative decrease of light emission under high injection current [30,31]. However, the Auger coefficients are hard to determine, since measurements are burdened by the influence of the e-h ratio, electric field, or hot carrier escape [32]. As a result, the Auger coefficients may vary by one or even two orders of magnitude [29]. Thus, there is an urgent demand of precise, independent assessment of the

contribution of Auger processes to e-h recombination, and the determination of the Auger coefficients.

The purpose of this work is to present a new method of analysis of the temporal evolution of the PL intensity, based on a logarithmic derivative method. The method allows the identification of the mono-, bi- and tri- molecular, and higher order PL decay processes. Examples of application are shown, demonstrating the power of the method. The perspectives of application in basic research and for the characterization of structures and devices are described.

II. THEORETICAL BACKGROUND

Time-resolved PL experiments proceed via excitement of the semiconductor sample by an intense laser pulse. The energy of the laser radiation is such that a photon can generate a single electron-hole (e-h) pair in the conduction and the valence band, respectively. The generated excess density of electrons $n(t_o)$ and holes $p(t_o)$ at the end of exciting pulse, t_o , is

$$n(t_o) = n_{tot}(t_o) - n_{eq} \quad (1a)$$

$$p(t_o) = p_{tot}(t_o) - p_{eq} \quad (1b)$$

where the suffixes ‘tot’ and ‘eq’ denote total and equilibrium density of the carriers, respectively. We assume that each photon generates an e-h pair, so that $n(t_o) = p(t_o)$. After the pulse, during the PL emission process ($t > t_o$), the e-h pairs are annihilated. Therefore, for negligible carrier escape, we can write $n(t) = p(t)$ for $t > t_o$.

The main *radiative recombination* process, which generates the PL signal, proceeds by band-to-band transitions involving an e-h pair, i.e. it is a bi-molecular process. Thus, the radiative recombination rate reflects the bi-molecular character of the process:

$$R_{rad}^b(t) = B^b n_{tot}(t) p_{tot}(t) \quad (2)$$

where B^b ($B^b > 0$) is a proportionality constant.

On the other hand, the recombination rate may also include radiative excitonic transitions and/or nonradiative *SRH recombination* related to the presence of the defects, when photogenerated carriers are captured at the defect site and then they gradually relax

towards the opposite band (ground state) by emission of phonons. These are a monomolecular processes described by recombination rate proportional to the excess carrier density, i.e.

$$R_{SRH}^b(t) = A^b n_{tot}(t) \quad (3)$$

where A^b ($A^b > 0$) is a proportionality constant associated to monomolecular process. Nonradiative SRH recombination is highly detrimental for the performance of optoelectronic devices, as it converts the absorbed energy into heat.

The third important recombination path, is *Auger recombination*, a tri-molecular process involving a photogenerated e-h pair and a third carrier (electron or hole) carrying out the excess energy. Therefore, the Auger recombination rate is given by

$$R_{Aug}^b(t) = C^{b1} n_{tot}^2(t) p_{tot}(t) + C^{b2} p_{tot}^2(t) n_{tot}(t) \quad (4)$$

where C^{b1} and C^{b2} are proportionality constants determined by the dynamics of Auger processes.

These three recombination paths contribute to the decrease of the excess carrier density, $n(t)$ and $p(t)$. Under high excitation, the excess densities are much higher than the equilibrium densities of both types of carriers. Therefore, for some initial period ($t > t_o$),

$$n_{tot}(t) \cong n(t) \quad (5a)$$

$$p_{tot}(t) \cong p(t) = n(t) \quad (5b)$$

In this case, the fundamental rate equation describing the optical relaxation, known as ABC equation, is

$$-\frac{dn}{dt} = R_{SRH}^b + R_{rad}^b + R_{Aug}^b = A^b n + B^b n^2 + C^b n^3 \quad (6)$$

The PL intensity $J_{PL}^b(t)$ is proportional to radiative recombination rate $R_{rad}^b(t)$:

$$J_{PL}^b(t) = \Gamma R_{rad}^b(t) = B^b n(t)^2 \Gamma \quad (7)$$

where Γ is the geometric factor of the photodetector. As the relevant information is contained in the time evolution, the PL intensity can be normalized to unity at the initial time t_o , i.e. $J_{PL}^b(t_o) = B^b n_o^2 \Gamma = 1$. Accordingly, Eq. (7) can be written as:

$$J_{PL}^b(t) = \left(\frac{n(t)}{n_o} \right)^2 \quad (9)$$

By division of Eq. (6) by initial carrier density $n(t_o) = n_o$:

$$-\frac{d}{dt} \left(\frac{n}{n_o} \right) = A^b \frac{n}{n_o} + B^b n_o \left(\frac{n}{n_o} \right)^2 + C^b n_o^2 \left(\frac{n}{n_o} \right)^3 \quad (10)$$

Multiplying of both sides of the equation by $2n(t)/n_o$ leads to the following expression for the time derivative of PL intensity:

$$-\frac{d}{dt} \left(\frac{n}{n_o} \right)^2 = -2 \frac{n}{n_o} \frac{dn}{dt} = -\frac{dJ_{PL}^b}{dt} = 2 \frac{n}{n_o} \left[A^b \frac{n}{n_o} + B^b n_o \left(\frac{n}{n_o} \right)^2 + C^b n_o^2 \left(\frac{n}{n_o} \right)^3 \right] \quad (11)$$

Finally, division by the PL intensity J_{PL}^b gives the final result

$$-\frac{1}{J_{PL}^b} \frac{dJ_{PL}^b}{dt} = -\frac{d}{dt} [\ln(J_{PL}^b)] = 2A^b + 2B^b n_o \sqrt{J_{PL}^b} + 2C^b n_o^2 J_{PL}^b \quad (12)$$

which allows a simple determination of the various contributions to carrier relaxation from an Arrhenius plot.

Note that Eq. (12) is only valid for high injection conditions. Therefore, a deviation from the equation is expected for $t > t_o$ when the excess carrier density decreases to a value comparable to equilibrium density of the dominant carrier type. The same situation arises when photogenerated carrier density is much lower than the density of majority carriers at equilibrium. In both cases the total density of majority carriers is approximately equal to equilibrium value, i.e. it is constant, independent of the time.

Under low injection conditions, the total carrier density under excitation can be approximated by:

$$n_{tot}(t) \approx n_{eq} \quad ; \quad p_{tot} = p(t) = n(t) \quad (15a)$$

when the majority carriers are electrons, and

$$p_{tot}(t) \approx p_{eq} \quad ; \quad n_{tot} = n(t) \quad (15b)$$

when the majority carriers are holes. Following Eq. (2), the radiative recombination rate can be approximated by

$$R_{rad}^m(t) = B^b n(t) n_{eq} = A^m n(t) \quad (16a)$$

or

$$R_{rad}^m(t) = B^b n(t) p_{eq} = A^m n(t) \quad (16b)$$

This means that the radiative recombination becomes monomolecular, governed by the excess density of the minority carriers. Note that for long enough time ($t \gg t_0$) the recombination process will always become monomolecular.

On the other hand, the SRH recombination contributes the monomolecular recombination rate, keeping proportional to the carrier density, i.e. $R_{SRH}^m(t) = A^b n(t)$ or $R_{SRH}^m(t) = A^b n(t)$, for electrons or holes as majority carriers, respectively.

Finally, the tri-molecular process, Auger recombination, is described by:

$$R_{Aug}^m(t) = C^m n_{eq}^2 n(t) = A_{Aug}^m n(t) \quad (18a)$$

when the majority carriers are electrons, and

$$R_{Aug}^m(t) = C^m n^2(t) p_{eq} = B_{Aug}^m n^2(t) \quad (18b)$$

when the majority carriers are holes. Hence, in the first case, the Auger recombination adds to monomolecular rate, and in the second it contributes to the bi-molecular recombination. Thus, for low injection, Eq. (6) becomes:

$$-\frac{dn}{dt} = R_{SRH}^m + R_{rad}^m + R_{Aug}^m = (A^b + A^m + A_{Aug}^m) n + B_{Aug}^m n^2 = A_{eff}^m n + B_{Aug}^m n^2 \quad (19)$$

As previously, the PL intensity $J_{PL}^m(t)$ is proportional to radiative recombination rate $R_{rad}^m(t)$ and the geometric factor Γ :

$$J_{PL}^m(t) = \Gamma R_{rad}^m(t) = A^m n(t) \Gamma \quad (20)$$

and the geometric factor Γ can be removed by normalizing PL intensity by its value at the initial time:

$$J_{PL}^m(t) = \frac{n(t)}{n_o} \quad (21)$$

Both sides of Eq. (19) are divided by n_o and by the PL intensity $J_{PL}^m(t)$ to arrive to the final expression:

$$-\frac{d[\ln(J_{PL}^m)]}{dt} = A_{eff}^m + B_{Aug}^m n_o J_{PL}^m \quad (22)$$

Note the similarity of the derived expression for high injection and low injection in Eqs (12) and (22), respectively. Therefore, it is possible to extract the coefficients associated with the different recombination processes from a common parabolic dependence:

$$F(y) = \alpha + \beta y + \lambda y^2 \quad (23)$$

where these factors depend on the type of the process:

$$- \text{ High injection: } y = \sqrt{J_{PL}^b}, \quad \alpha = 2A^b, \quad \beta = 2B^b n_o, \quad \lambda = 2C^b n_o^2 \quad (24a)$$

$$- \text{ Low injection: } y = J_{PL}^m, \quad \alpha = A_{eff}^m, \quad \beta = B_{Aug}^m n_o, \quad \lambda \approx 0 \quad (24b)$$

As shown in Fig. 1 (a), the high injection regime (labeled as a process I) evolves towards low injection (labeled as process II), characterized by linear dependence of PL intensity, i.e. Eq. (14) relation is not fulfilled. Using the relation $J_{PL}^m = K(\sqrt{J_{PL}^b})^2$, the following dependence is obtained:

$$-\frac{d[\ln(J_{PL}^m)]}{dt} = A + B n_o K (\sqrt{J_{PL}^b})^2 + C n_o^2 K^2 (\sqrt{J_{PL}^b})^4 \quad (25)$$

i.e. in the part of diagram corresponding to Process II, plotted in Fig. 1a, the dependence on $\sqrt{J_{PL}^b}$ should be bi-quadratic.

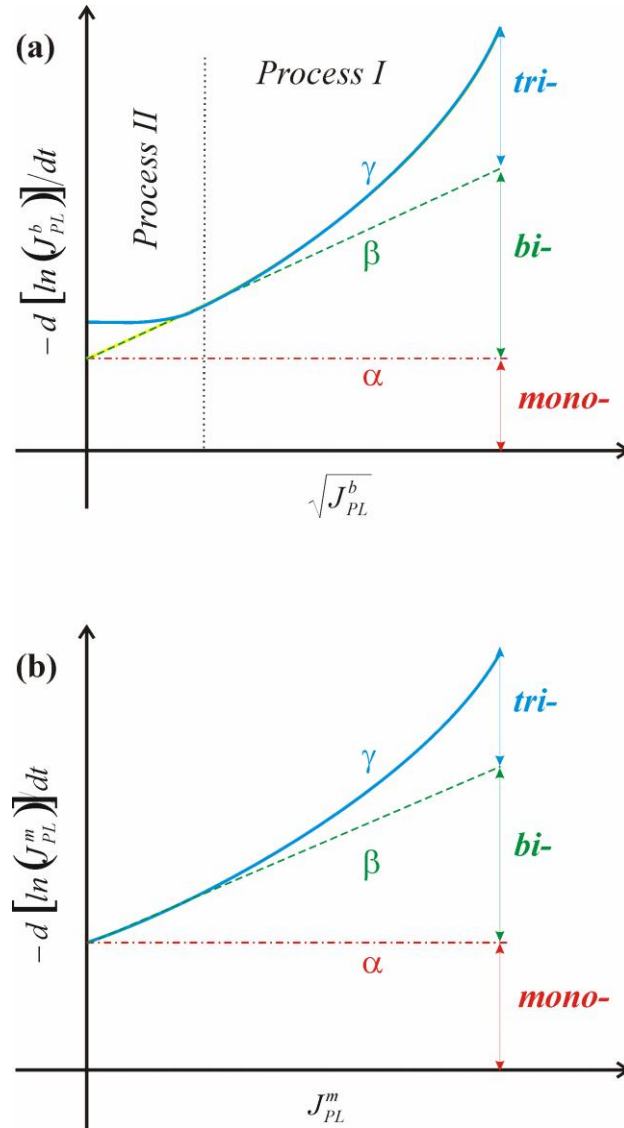


Fig. 1. Logarithmic time derivative of PL intensity for two different excitation levels: (a) for high excitation, as a function of square root of PL intensity, and (b) for low excitation, as a function of PL intensity. In (a), the high excitation regime is divided by vertical dotted line into process I (Eq. (23)) and process II (Eq. (26)). The red dash-dotted, green dotted and solid blue line correspond to the evolution according to α , $\alpha + \beta$ and $\alpha + \beta + \gamma$ parameters. The values of the parameters are: $\alpha = 1$, $\beta = 2$ and $\gamma = 3$. The relative weight of the various molecular processes at the initial level is marked by arrows for $J = 1$.

Note that the implementation of the above presented procedure requires satisfying several stringent conditions. First, the averaged PL intensity should drop to zero for long enough times. Finally, it has to be stressed that the ABC model is a mere approximation of the more complex phenomena of optical relaxation, so that a deviation is likely to be detected.

III. APPLICATION TO GaN/AlN MULTI-QUANTUM-WELLS

As an example, we present here the analysis of the TRPL from a polar GaN/AlN multi-quantum-well (MQW) structure grown on an AlN-on-sapphire substrate by plasma-assisted molecular beam epitaxy (PA-MBE). The MQW stack consists of 40 periods of 1.0-nm-thick GaN wells and 4-nm-thick AlN barriers. The GaN layers were doped with Si to a concentration of $1.3 \times 10^{19} \text{ cm}^{-3}$. A scanning transmission electron microscopy (TEM) view of the MQW is presented in Fig. 2. The picture proves that the thicknesses of barrier/wells are almost uniform with low density of extended defects.

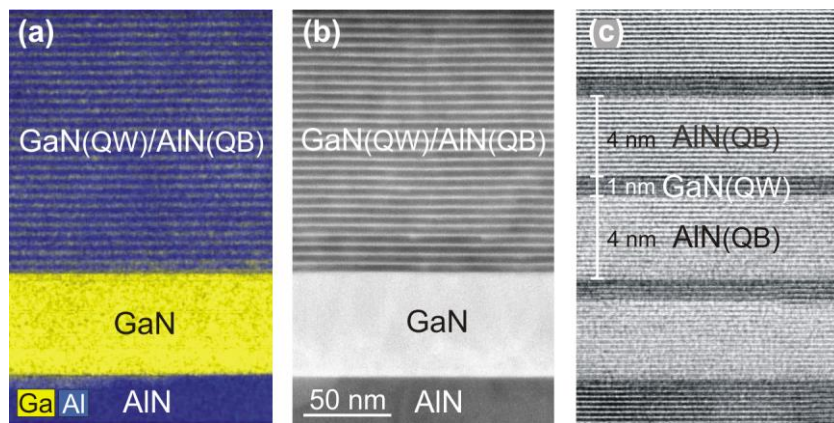


Fig. 2. Cross-sectional HAADF-STEM image of 1-nm-thick GaN wells with 4 nm-thick AlN barriers the GaN/AlN MQW structure: (a) EDX map of chemical composition of the structure, (b) HAADF map, (c) high-resolution TEM image.

The choice of such narrow GaN wells aims at neglecting the effect of the polarization-related internal electric field on the evolution of the radiative recombination. In polar GaN/AlN heterostructures, the quantum-confined Stark effect (QCSE) leads to a red shift of the PL. Just after the excitation pulse, the electric field in polar QWs is partially screened by photoexcited carriers, what causes an initial increase of the emission energy (blue shift of the PL). Then, the recombination reduces screening, and the electric field is rebuilt resulting in a red shift as a function of time. Naturally, QCSE is less pronounced for narrow structures.

The use of nonpolar crystallographic orientations allows for GaN/Al(Ga)N systems to operate without polarization-induced electric field [33], which simplifies the interpretation of TRPL data. As an example, we have characterized a nonpolar m-plane MQW stack consisting of 50 periods of 3.0-nm-thick GaN wells and 26-nm-thick $\text{Al}_{0.26}\text{Ga}_{0.74}\text{N}$ barriers. The GaN layers were doped with Si to a concentration of $2 \times 10^{19} \text{ cm}^{-3}$. The samples were grown by PAMBE at a substrate temperature $T_S = 720^\circ\text{C}$ and with a nitrogen-limited growth rate of 0.4 ML/s ($\approx 360 \text{ nm/h}$). Growth was performed under slightly Ga-rich conditions [34, 35]. The substrate was free-standing semi-insulating GaN sliced along the m-plane nonpolar surface from (0001)-oriented GaN boules synthesized by hydride vapor phase epitaxy (resistivity $>10^6 \Omega\text{cm}$, dislocation density $<5 \times 10^6 \text{ cm}^{-2}$).

Photoluminescence was excited with the third harmonic of a Ti:sapphire pulsed laser ($\lambda = 300 \text{ nm}$, $f = 80 \text{ MHz}$, pulse width 130 fs). The laser average power was up to 1 mW, impulse energy 12.5 pJ. The light beam was analyzed by spectrometer and directed on a CCD detector and a streak camera. The streak camera enabled time-resolved measurements, showing the time evolution of PL intensity and energy.

As shown in Fig 3a, the PL spectra from 1-nm-thick polar GaN/AlN QWs show no discernible energy shift in time. The energy is constant because the well is so narrow that the screening does not affect the quantum states during the recombination process. Similar time independent emission energy measured for the 3-nm-thick nonpolar GaN/ $\text{Al}_{0.26}\text{Ga}_{0.74}\text{N}$ QWs is presented in Fig 3b.

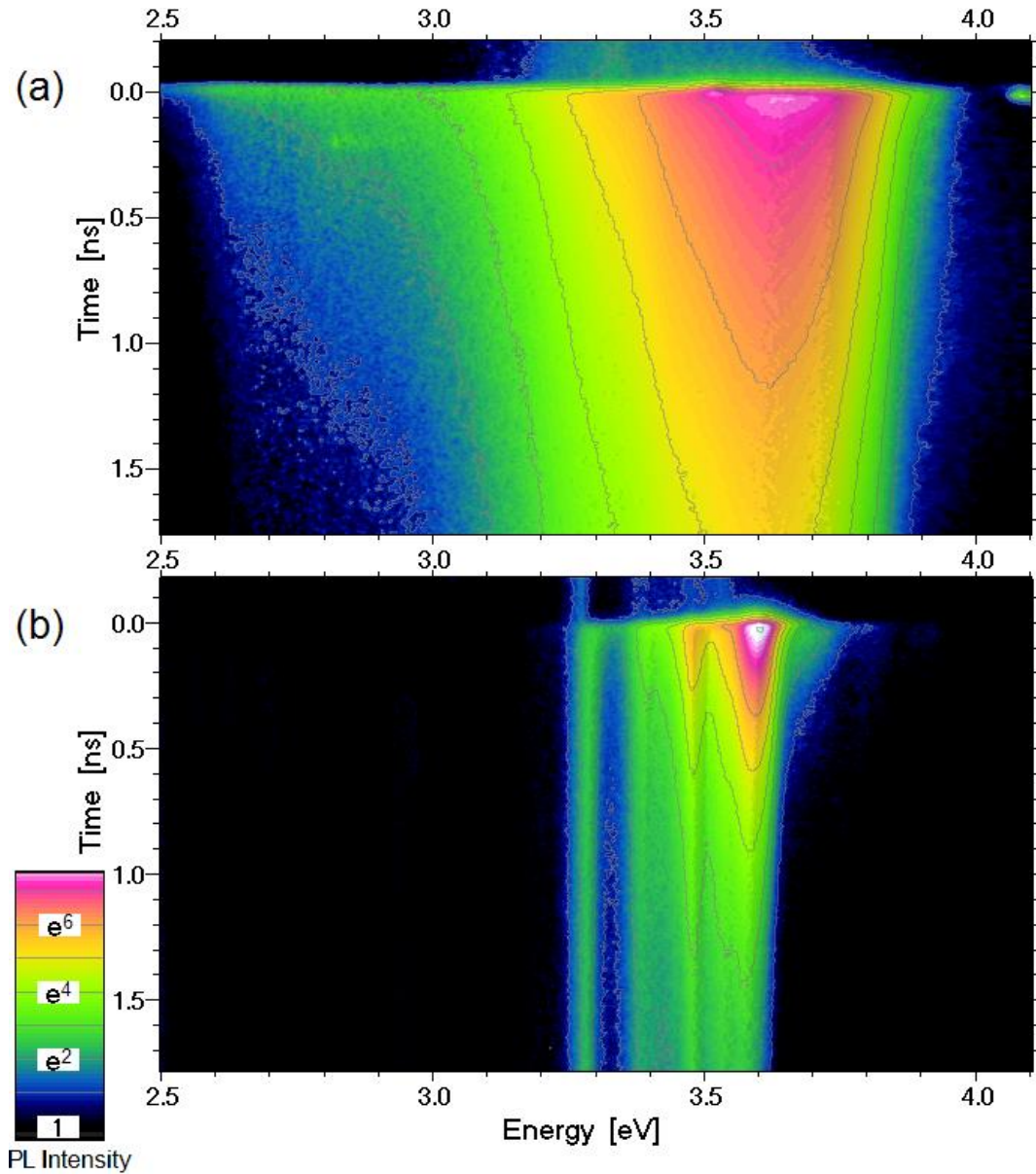


Fig 3. Time-resolved PL spectra of (a) polar 1-nm-thick GaN/AlN MQWs and (b) nonpolar 3-nm-thick GaN/Al_{0.26}Ga_{0.74}N MQWs. Contour lines are equally spaced in logarithmic scale (e – times spaced), so distance between two contour lines along time axis gives the decay time of the signal.

The logarithmic plot of PL intensity of polar nitride MQW structure versus time is shown in Fig. 4 (a) and (b) for room and liquid-helium temperatures, respectively. In addition to raw data, the data obtained by subtraction of the background value at infinity is shown. For long decay times, the PL extinction is exponential.

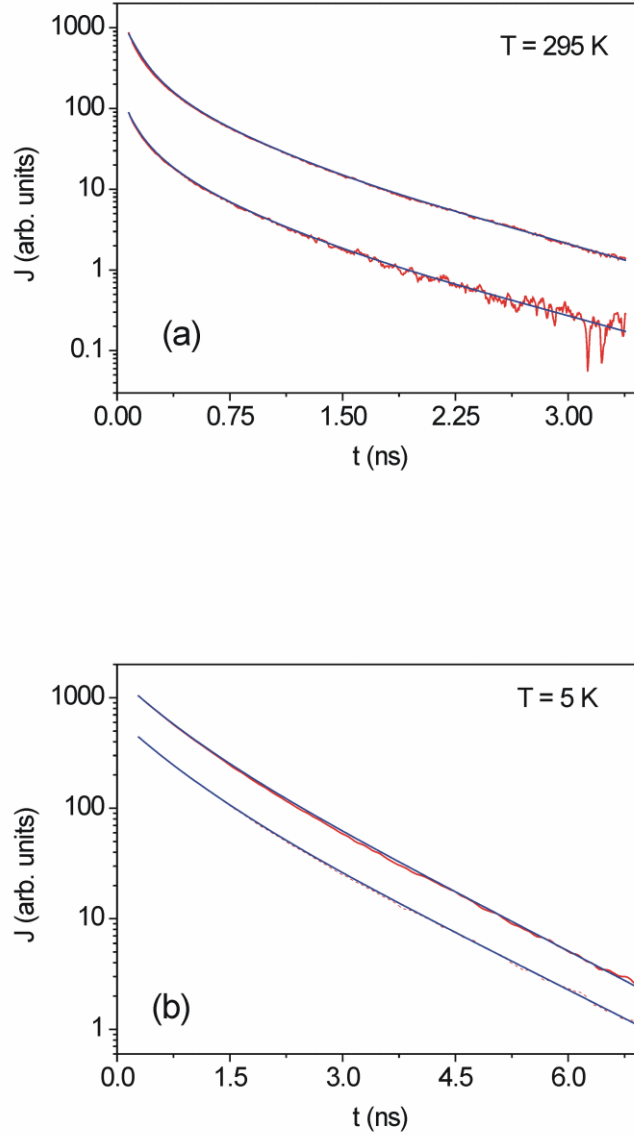


Fig 4. PL time decay of polar nitride MQW structure collected at 295K (a) and 5K(b) in the (3.37 eV, 3.90 eV) energy interval. The red line denotes raw signal with the background subtracted, the blue line – noise averaged line. The dominant emission peaks were located within this interval during entire measurement time (see the spectrum in Fig. 3a). The laser power was 1000 and 100 μW , and 500 and 200 μW for high and low temperature, respectively. The excitation wavelength was 300 nm.

The noise level was reduced by the following method: the smoothing interval was selected as a given odd number of points. Then according to least square method the linear approximation to the data in the interval was obtained. The central value was adopted as new value, replacing the old one. The procedure was repeated consecutively for all points along

the line. At both ends, the data remain unchanged. As the noise to signal ratio was different for different times, the smoothing interval was different at both ends, equal to N_{\max} and N_{\min} , respectively. For the points between the smoothing interval length was scaled using the noise to the signal ratio, defined as

$$q \equiv \frac{\sqrt{\sum (j_i - j_{av})^2}}{j_{av} N_{\min}} \quad (26a)$$

where the average value is given as standard mean:

$$j_{av} \equiv \frac{1}{N_{\min}} \sum_{N_{\min}} j_i \quad (26b)$$

The interval length was obtained from the linear scaling:

$$N = N_{\min} + \frac{(N_{\max} - N_{\min})(q - q_{\min})}{(q_{\max} - q_{\min})} \quad (27)$$

The procedure was repeated several times to obtain sufficient smoothing. For instance, for low temperature data (5K) obtained with an average laser power of 500 and 200 μW , the smoothing integral begins at for one point (i.e. efficiently no smoothing) and terminates at 81 and 121 points, respectively. The procedure was repeated 3 and 5 times respectively which was sufficient to remove the noise so that the derivative could be obtained. It has to be stressed out that the number of points in smoothing interval and the number of iterations has to be drastically changed depending on the noise/signal ratio.

From the smoothed time dependence, the logarithmic derivative of the PL intensity $-\frac{d[\ln(J)]}{dt}$ as a function of the intensity J were obtained. It has to be noted that the initial time dependence does not obey ABC dynamics, evidently due to electron and hole transportation/equilibration processes. Therefore the plotted diagram corresponds to the terminating phase of the evolution where the system remains in local equilibrium.

With the used laser power we estimate a photo-generated carrier density in the range of 10^{16} cm^{-3} . Thus, at room temperature, in the samples under study, the density of photo-generated carriers is expected to be lower than the equilibrium density of majority carriers coming from Si donors [36]. Therefore, the PL intensity is proportional to the excess density

of minority carriers as in the low injection regime described by Eq. 4(b), and a linear dependence is expected, as confirmed by the fit in Fig 5(a). For low temperature $T = 5K$, the majority carriers are thermalized [36], and their density is small compared to the photo-generated density of the carriers. In such a case the PL intensity is assumed to be proportional to the density of both carrier types, electrons and holes, thus effectively proportional to the square of the new carrier density. Therefore the low temperature PL intensity is plotted in function of the square root of PL intensity in Fig. 5(b). Both diagrams are scaled to the initial PL intensity, i.e. the following dependence is used:

$$F(y) = \alpha + \beta y + \lambda y^2 \quad (28)$$

where $y = \frac{J}{J(t_o)}$ and $y = \frac{J^{1/2}}{J^{1/2}(t_o)}$ for Fig. 5(a) and Fig. 5(b) respectively.

As it is shown, for high temperature measurements the PL intensity scales linearly with the independent variable. The diagrams obtained for laser power $L = 1000 \mu W$ and $L = 100 \mu W$ are approximately identical. From the linear approximation, the following data may be derived: the coefficient α determining the monomolecular process is $\alpha^m = A^m = 1.49 ns^{-1}$. Thus the linear relaxation time is $\tau^m = 0.67 ns$. The coefficient β is: $\beta^m = B^m n_o = 4.55 ns^{-1}$. Assuming that the initial density is approximately $n_o \cong 1.06 \times 10^{16} cm^{-3}$ the value of B^m parameter is $B^m \cong 4.29 \times 10^{-13} m^{-3} s^{-1}$. As it is shown the third order term is negligible. It may be also observed that the linear dependence is strictly followed by experimental data for $L = 100 \mu W$ while the higher power data show weak square root behavior. Thus, it may be deduced that the high laser power excitation $L = 1000 \mu W$ generates number of additional carriers which is relatively high, but only slightly affecting the density of majority carriers.

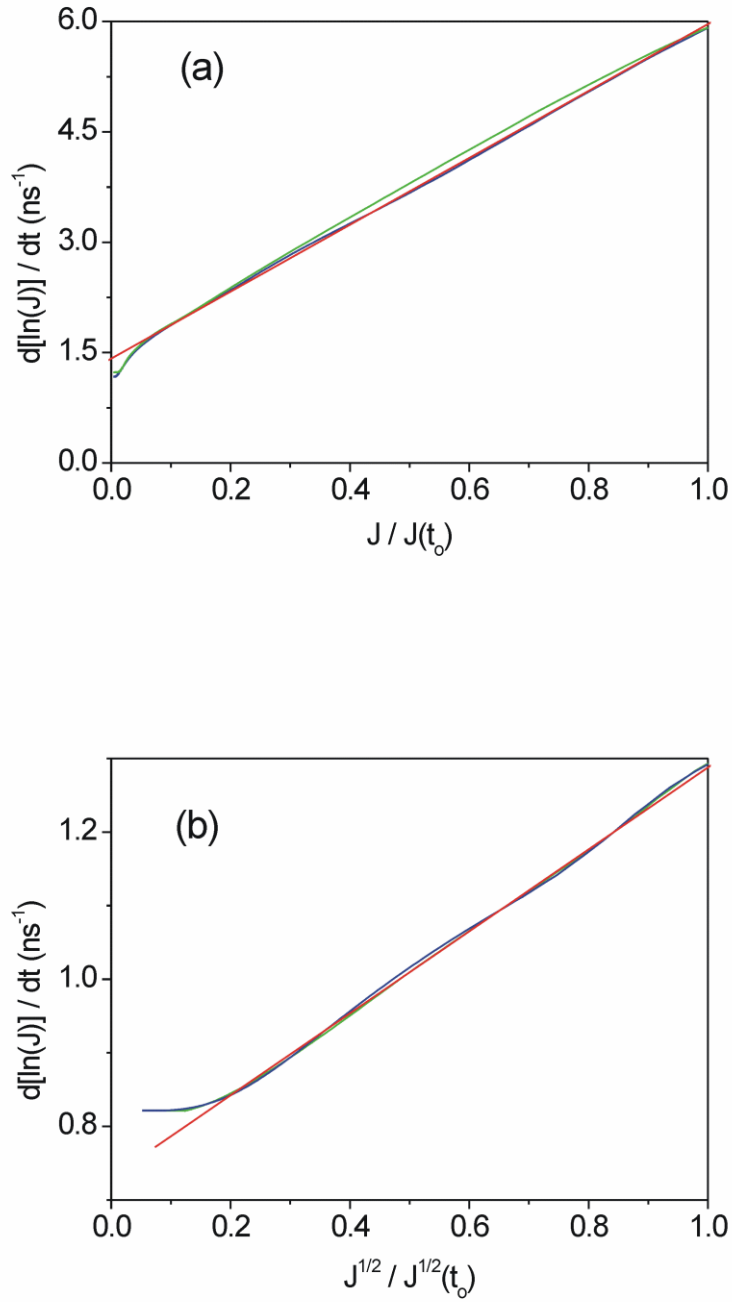


Fig. 5. Logarithmic time derivative as a function of the intensity of the normalized PL intensity from polar nitride MQW structure at room temperature (a) and 5 K (b). The room temperature diagram (a) presents the data for laser power $L = 1000 \mu\text{W}$ (green line) and $L = 100 \mu\text{W}$ (blue line) and linear approximation (red line). The low temperature diagram (b) presents the data for laser power $L = 500 \mu\text{W}$ (green line) and $L = 200 \mu\text{W}$ (blue line) and linear approximation (red line).

The low temperature data definitely show square root dependence for most of the diagram presented in Fig. 5 (b). From the linear fit in the figure, we obtain the coefficient α as $\alpha^b = 2A^b = 0.73 \text{ ns}^{-1}$, so that the relaxation time is $\tau^b = 2.74 \text{ ns}$. The coefficient β is: $\beta^b = 2B^b n_o = 0.56 \text{ ns}^{-1}$. Again assuming the initial density $n_o \cong 1.1 \times 10^{16} \text{ cm}^{-3}$ the value of B^b parameter is $B^b \cong 2.55 \times 10^{-14} \text{ m}^{-3} \text{ s}^{-1}$. Thus the coefficients A and B are much lower for bimolecular recombination. The nonlinear Auger related contribution is negligible in both cases. For low PL intensity, the dependence is bi-quadratic as predicted in Fig. 1(a), thus confirming the overall picture of the process.

The polar MQW are affected by built-in and piezo-induced internal electric affecting electrons and hole. Therefore it is also interesting to investigate nonpolar MQWs. For comparison we present high and low temperature TRPL data obtained from equally 4 nm wide AlN/GaN MQWs structure. The time evolution is presented in Fig. 6.

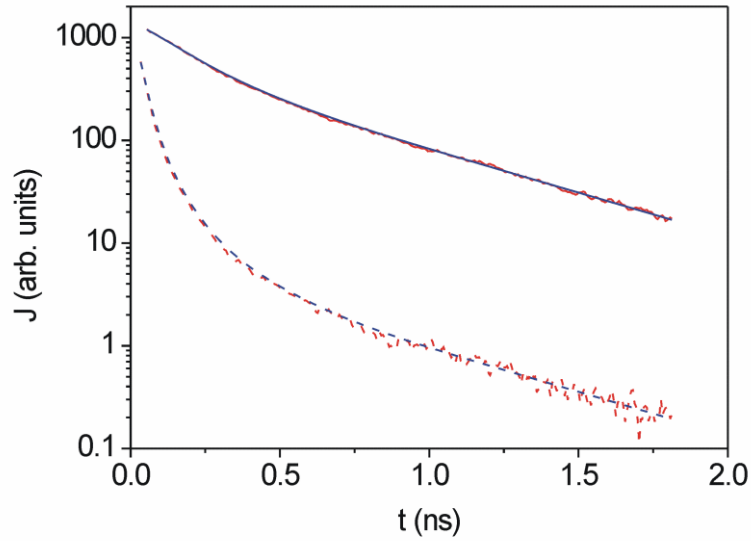


Fig. 6. PL time decay of nonpolar nitride MQW structure collected at 300K (dashed lines) and 5K (solid lines) in the (3.3738 eV, 3.8978 eV) energy interval. The red line denotes raw signal with the background subtracted, the blue line – noise averaged line. The dominant emission peaks were located within this interval during entire measurement time. The laser power was 500 μW and the wavelength was 300 nm.

From these data it follows again that the long time evolution is exponential, similar to the data obtained for narrow polar QWs. Thus for 1 nm wells, the electric field do not play important role as predicted on the time - independent PL emission energy.

As before, the analysis could be made using Eqs 12 and 19 so that the logarithmic time derivative of PL intensity can be obtained after application of appropriate smoothing procedure. The results are presented in Fig. 7.

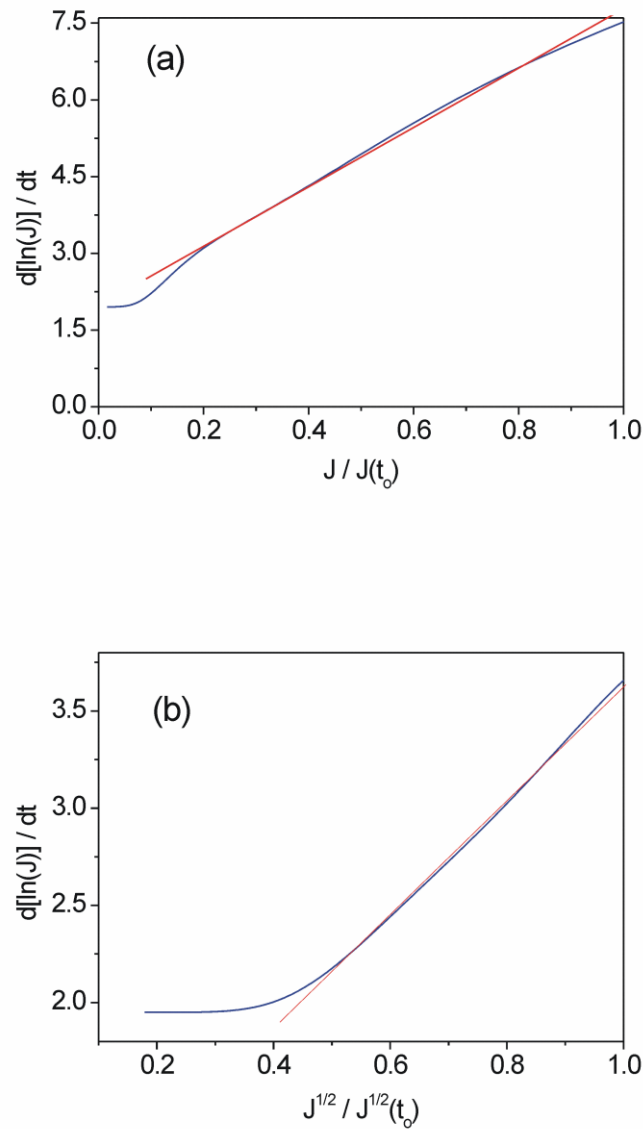


Fig. 7. Logarithmic time derivative as a function of the intensity of the normalized PL intensity from polar nitride MQW structure at 300 K (a) and 6 K (b): measured data (blue line) and linear approximation (red line).

As expected, high temperature data could be approximated by linear dependence while the helium temperature data are governed by square root dependence. From the linear approximation the following data may be derived for 300 K: the coefficient α determining the monomolecular process is $\alpha^m = A^m = 1.97 \text{ ns}^{-1}$. Thus the linear relaxation time is $\tau^m = 0.51 \text{ ns}$. The coefficient β is: $\beta^m = B^m n_o = 5.80 \text{ ns}^{-1}$. Assuming that the initial density is approximately $n_o \cong 2.6 \times 10^{14} \text{ cm}^{-3}$ the value of B^m parameter is $B^m \cong 2.23 \times 10^{-10} \text{ m}^{-3} \text{ s}^{-1}$. The data for low temperature follow square dependence. The coefficient α is: $\alpha^b = 2A^b = 0.69 \text{ ns}^{-1}$ which is translated to the relaxation time: $\tau^b = 2.9 \text{ ns}$. The the coefficient β is: $\beta^b = 2B^b n_o = 2.93 \text{ ns}^{-1}$. Assuming that the initial density is approximately $n_o \cong 8.3 \times 10^{15} \text{ cm}^{-3}$ the value of B^b parameter is: $B^b \cong 1.77 \times 10^{-13} \text{ m}^{-3} \text{ s}^{-1}$.

From these data, narrow-well polar and nonpolar MQWs PL show remarkable similarity. Note that despite identical growth conditions, due to the different crystallographic orientation, the point defect density may be different inducing some difference in the PL data.

IV. SUMMARY

We have presented a new method of analysis of TRPL data, based on the dependence of logarithmic time derivative of the PL intensity as a function of the same PL intensity. The transformation of the TRPL data is exact, avoiding any approximations. The application of the method is universal, it could be used to analyze the PL decay kinetics of any system, including semiconducting, molecular etc. The method provides graphic representation of the results allowing identification of the mono, bi-, tri-molecular and higher order recombination processes. Therefore the method could be used to determine standard ABC constants. Successful application of the method requires two conditions to be met: efficient noise reduction scheme and the precise determination of the zero signal level. The procedures describing how attain these two goals were also presented.

The presented method was used to identify the value of the monomolecular A parameter, the bi-molecular B parameter, and negligible contribution of higher order processes, including Auger recombination in the exemplary polar and nonpolar GaN/AlN MQW systems. Potentially, the method may precisely verify various models of the efficiency droop in the nitride devices.

Acknowledgements

This research was supported by the Polish National Science Center grant number DEC-2015/19/B/ST5/02136. The TEM study was carried out at the CNBCh UW, established within the project co-financed by EU from the European Regional Development Fund under the Operational Programme Innovative Economy, 2007 – 2013 and NCBR Panda2 501-D312-56-0000002.

REFERENCES

- [1] G.F.J. Garlic, *Luminescence*, in *Light and Matter II*, G. Flugge (ed), Springer-Verlag, Berlin-Heidelberg 1958, p. 1.
- [2] V.H.B. Bebb, and E.W. Williams, *Photoluminescence I. Theory*, in *Semiconductors and Semimetals*, R.K. Willardson and A. C. Beer (eds), Academic Press, New York 1972, Vol. 8, p. 181.
- [3] V. P. Gribkovskii, *Theory of Luminescence*, in *Luminescence of Solids*, D. R. Vij (ed), Plenum Press, New York, 1998.
- [4] I. Pelant, J. Valenta, *Luminescence Spectroscopy of Semiconductors*, Oxford Univ. Press, Oxford, 2012.
- [5] S. M. Sze, *Physics of Semiconductor Devices*, Wiley, New York, 2001.
- [6] W. Shockley, W. T. Read, Jr. *Phys. Rev.* **87**, 835 (1952).
- [7] G.H. Wannier, *Phys. Rev.* **52**, 191 (1937).
- [8] N. F. Mott, *Trans. Faraday Soc.* **34**, 500 (1938).
- [9] M. H. Anderson, J. R. Ensher, M. R. Matthews, C. E. Wieman, and E. A. Cornell, *Science*, **269**, 198 (1995).

- [10] S. Schmitt-Rink, D.S. Chemla, and D. A. B. Miller, *Phys. Rev. B.* **32**, 6601 (1985).
- [11] E. Zielinski, F. Keppler, S. Hausser, M. H. Pilkuhn, R. Sauer, and W. T. Tsang, *IEEE J. Quant. Electron.* **25**, 1407 (1989).
- [12] M. F. Schubert, S. Chhajed, J. K. Kim, E. F. Schubert, D. D. Koleske, M. H. Crawford, S. R. Lee, A. J. Fischer, G. Thaler, and M. A. Banas, *Appl. Phys. Lett.* **91**, 231114 (2007)
- [13] Q. Dai, Q. Shan, J. Weng, S. Chhajed, J. Cho, E. F. Schubert, M. H. Crawford, D. D. Koleske, M.-H. Kim, and Y. Park, *Appl. Phys. Lett.* **97**, 133507 (2010).
- [14] M. G. Brik, S. Mahlik, D. Jankowski, P. Strak, K. P. Korona, E. Monroy, S. Krukowski, and A. Kaminska, *Jpn. J. Appl. Phys.* **56**, 05FA02 (2017).
- [15] F. Wootan, *Optical Properties of Solids*, Academic Press, New York, 1972.
- [16] M. Inokuti and F. Hirayama, *J. Chem. Phys.* **43**, 1978 (1965).
- [17] M. Millot, Z. M. Geballe, K. M. Yu, W. Walukiewicz, and R. Jeanloz, *Appl. Phys. Lett.* **100**, 162103 (2012).
- [18] S. Chichibu, T. Azuhata, T. Sota, S. Nakamura, *Appl. Phys. Lett.* **69**, 4188, (1996).
- [19] S. Chichibu, T. Azuhata, T. Sota, S. Nakamura, *Appl. Phys. Lett.* **70**, 2822 (1997).
- [20] S. F. Chichibu, A. Uedono, T. Onuma, B. A. Haskell, A. Chakraborty, T. Koyama, P. T. Fini, S. Keller, S. P. Denbaars, J. S. Speck, U. K. Mishra, S. Nakamura, S. Yamaguchi, S. Kamiyama, H. Amano, I. Akasaki, J. Han, T. Sota, *Nature Mater.* **5**, 810 (2006).
- [21] R. A. Oliver, S. E. Benett, T. Zhu, D. J. Beesley, M. J. Kappers, D. W. Saxey, A. Cerezo, C. J. Humphreys, *J. Phys. D: Appl. Phys.* **43**, 354003 (2010).
- [22] F. Bernardini, V. Fiorentini, and D. Vanderbilt, *Phys. Rev. Lett.* **79**, 3958 (1997).
- [23] A. Kaminska, P. Strak, J. Borysiuk, K. Sobczak, J. Z. Domagala, M. Beeler, E. Grzanka, K. Sakowski, S. Krukowski, E. Monroy, *J. Appl. Phys.* **119**, 015703 (2016).
- [24] P. Strak, P. Kempisty, K. Sakowski, A. Kaminska, D. Jankowski, K. P. Korona, K. Sobczak, J. Borysiuk, M. Beeler, E. Grzanka, E. Monroy and S. Krukowski, *AIP Advances* **7**, 015027 (2017).
- [25] P. Strak, P. Kempisty, K. Sakowski, and S. Krukowski, *J. Cryst. Growth* **401**, 652 (2014).
- [26] A. Suchocki, J. M. Langer, *Phys. Rev. B* **39**, 7905 (1989).
- [27] S. Hausser, G. Fuchs, A. Hangleiter, K. Streubel, and W. T. Tsang, *Appl. Phys. Lett.* **56**, 913 (1990).
- [28] J. Cho, E. Schubert, and J. Kim, *Laser Photon. Rev.* **7**, 408 (2013).

- [29] M. Shahmohammadi, W. Liu, G. Rossbach, L. Lahourcade, A. Dussaigne, C. Bougerol, R. Butte, N. Grandjean, B. Deveaud, and G. Jacopin, *Phys. Rev. B* **95**, 125314 (2017).
- [30] M. R. Krames, G. Christenson, D. Collins, L. W. Cook, M. G. Craford, A. Edwards, R. M. Fletcher, N. F. Gardner, W. K. Goetz, W. R. Imler, E. Johnson, R. S. Kern, R. Khare, F. A. Kish, C. Lowery, M. J. Ludowise, R. Mann, M. Maranowski, S. A. Maranowski, P. S. Martin *et al.*, *Proc. SPIE* **3938**, 2 (2000).
- [31] T. Mukai, M. Yamada, and S. Nakamura, *Jpn. J. Appl. Phys.* **38**, 3976 (1999).
- [32] J. Piprek, F. Roemer, and B. Witzigmann, *Appl. Phys. Lett.* **106**, 101101 (2015).
- [33] J.S. Speck and S. F. Chichibu, *MRS Bulletin*, **34**, 304 (2009).
- [34] C. B. Lim, A. Ajay, and E. Monroy, *Appl. Phys. Lett.* **111**, 022101 (2017).
- [35] C. B. Lim, M. Beeler, A. Ajay, J. Lähnemann, E. Bellet-Amalric, C. Bougerol, and E. Monroy, *J. Appl. Phys.* **118**, 014309 (2015).
- [36] V. Bougrov, M.E. Levinshtein, S.L. Rumyantsev, A. Zubrilov, in *Properties of Advanced Semiconductor Materials GaN, AlN, InN, BN, SiC, SiGe*. Eds. M.E. Levinshtein, S.L. Rumyantsev, M.S. Shur, John Wiley & Sons, Inc., New York, 2001, 1-30.